

# 2 Theoretical Analysis and Determination of the 3 Correction Factor for a Waveguide Microcalorimeter

4 Xiaohai Cui <sup>1,\*</sup>, Yu Song Meng <sup>2</sup>, Wenze Yuan <sup>1</sup> and Yong Li <sup>1</sup>

5 <sup>1</sup> National Institute of Metrology, Beijing 100013, China; cuixh@nim.ac.cn

6 <sup>2</sup> National Metrology Centre, Agency for Science, Technology and Research (A\*STAR), Singapore 118221,  
7 Singapore; ysmeng@ieee.org, meng\_yusong@nmc.a-star.edu.sg

8 \* Correspondence: cuixh@nim.ac.cn; Tel.: +86-10-6452-5221

9 Received: date; Accepted: date; Published: date

10 **Abstract:** This paper proposes a new method for determining the correction factor of a newly  
11 developed waveguide primary power measurement system (i.e., microcalorimeter), based on the  
12 electromagnetic field theory analysis for waveguide thermal isolation section (TIS) in foil short  
13 measurement mode. The new method determines the contribution of the power dissipated within  
14 the TIS into the correction factor, in term of the physical dimensions of the TIS. Performance  
15 comparison and analysis show that the newly proposed method can significantly reduce the  
16 measurement uncertainty when evaluating the correction factor of waveguide microcalorimeters.

17 **Keywords:** correction factor; electromagnetic field theory; microcalorimeter; primary standards  
18

---

## 19 1. Introduction

20 Microcalorimeter has been recognized to be an effective solution for RF, microwave and  
21 millimeter-wave power measurements [1-3], and have been successfully developed within the  
22 National Metrology Institutes world-widely over past few decades [4-8]. The main function and  
23 application of a microcalorimeter is to determine the effective efficiency  $\eta_e$  of a transfer standard  
24 (e.g., a thermistor mount, and referred as a Device Under Test [DUT] in this paper), and its correction  
25 factor  $g$  is found to be critical and has been studied in many different ways [9-12].

26 In the millimeter-wave range, waveguide microcalorimeter has been adopted due to its good  
27 reliability and accuracy up to 110 GHz [8, 10-12] or further. In order to accurately determine its  
28 correction factor  $g$ , a method based on the measurement of offset shorts of different length followed  
29 by one single calibration measurement of a DUT has been proposed in [10]. Recently, another method  
30 based on attaching a thermistor sensor into the waveguide thermal isolation section (TIS) to  
31 accurately measure its temperature change has been proposed in [12]. Both the methods are found to  
32 have good performance during the evaluations of a WR-22 (33-50 GHz) waveguide microcalorimeter.

33 However as the frequency of interest further increases, the size of waveguide becomes smaller  
34 which motivates us to find other solutions without using extra fixtures/accessories. As a continued  
35 work of [13], theoretical analysis and modeling of the correction factor  $g$  of a waveguide  
36 microcalorimeter will be performed in this paper, in term of the physical dimensions of its TIS, based  
37 on the electromagnetic field theory analysis. The proposed solution tends to eliminate the usage of  
38 external fixtures, and reduce the measurement uncertainty when calibrating a RF/microwave/  
39 millimeter-wave power sensor with waveguide connection. For simplicity in the rest of this paper,  
40 RF will be synonymous for RF, microwave, and millimeter-wave.

41 In the remaining of this paper, theoretical background and operation principle of a waveguide  
42 microcalorimeter will be discussed in Section 2. This is followed by the proposal of a new method for  
43 determining its correction factor  $g$  in Section 3. In Section 4, detailed description of electromagnetic  
44 field theory analysis for waveguide TIS in foil short measurement mode will be carried out.

45 Performance comparison of the new method will be given in Section 5. Finally, conclusion of this  
 46 paper will be drawn in Section 6.

## 47 2. Theoretical Background and Operation Principle

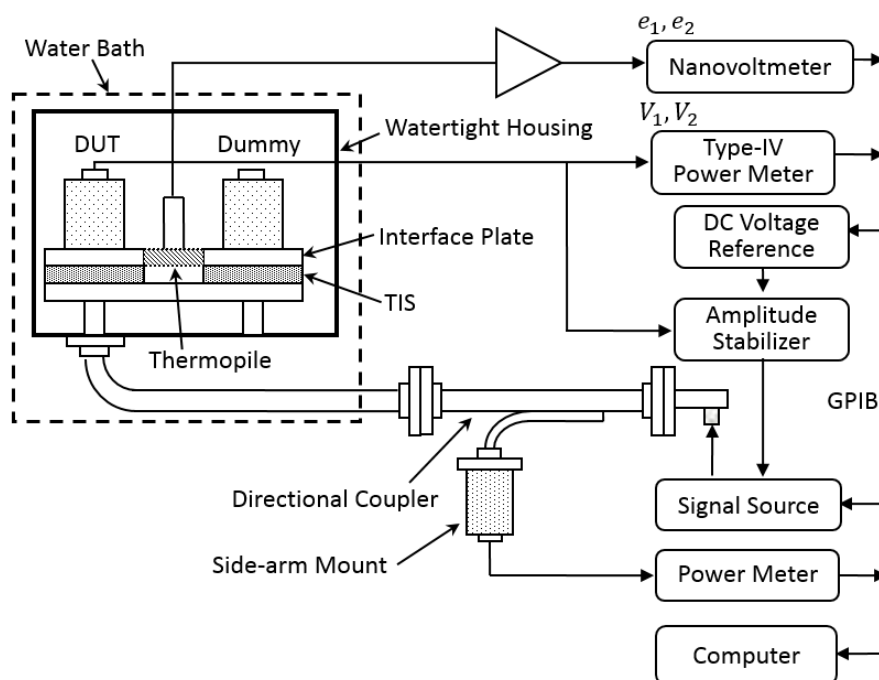
48 The effective efficiency  $\eta_e$  of a thermistor mount (a type of power sensor which is widely used  
 49 for precision RF power measurements) is important for accurate determination of total power  $P_{rf}$   
 50 dissipated within the thermistor mount, and is defined as

$$51 \quad \eta_e = \frac{P_{sub}}{P_{rf}}. \quad (1)$$

52 where  $P_{sub}$  is the direct current (dc) substituted power of the thermistor mount and calculated in  
 53 term of its bias voltages without and with RF signal applied (i.e.,  $V_1$  and  $V_2$ ) at a steady status as  
 54 follows;

$$55 \quad P_{sub} = \frac{V_1^2 - V_2^2}{R}. \quad (2)$$

56 Here,  $R$  is the operating resistance of the thermistor mount. Figure 1 below shows a detailed  
 57 measurement setup for determining the effective efficiency  $\eta_e$  of a DUT thermistor mount. Its core  
 58 part consists of a thermally insulated microcalorimeter (twin-line structure) including a thermopile  
 59 and a thermal reference (dummy), and a Type-IV power meter.  $V_1$  and  $V_2$  are measured by the Type-  
 60 IV meter directly.  
 61



62  
 63 **Figure 1.** Schematic diagram for the setup and operation of a waveguide microcalorimeter.

64 According to the *law of conservation of energy*, the unsubstituted portion (labeled as  $P_w$ , and  $P_{rf} =$   
 65  $P_{sub} + P_w$ ) of total dissipated power  $P_{rf}$  can cause relative temperature rise of the DUT mount  
 66 referring to the Dummy mount which is monitored by the thermopile as shown in Figure 1, and  
 67 supposed to be indicated by thermopile output voltage change  $\Delta e = e_2 - e_1$ , where  $e_1$  and  $e_2$  are the  
 68 output voltages of the thermopile corresponding to  $V_1$  and  $V_2$  and measured by a nanovoltmeter. It  
 69 is noted that this unsubstituted power  $P_w$  is the portion of RF power dissipated but does not affect  
 70 the reading  $V_2$  of the nanovoltmeter.

### 71 2.1. Definition of the Correction Factor

72 However, the power  $P_i$  dissipated at its waveguide TIS can also contribute to  $\Delta e$ , and therefore  
 73 has to be differentiated. Without differentiation, the output voltage change  $\Delta e$  of thermopile  
 74 includes the contribution from  $P_w$  and  $P_i$ , with the following relationship,

$$75 \quad \Delta e = k(P_w + cP_i), \quad (3)$$

76 where  $k$  is a proportionality constant that depends on the fraction of power that is detectable by the  
 77 thermopile and the thermopile sensitivity [11], and  $c$  is an equivalence factor that considers the  
 78 thermal paths which are different comparing to those from the mount to the thermopile.

79 The uncorrected effective efficiency  $\eta_{e,uncor}$  [7] comparing to the effective efficiency  $\eta_e$  in (1),  
 80 including the contribution from  $P_i$  to the thermopile output voltage change  $\Delta e$ , and is defined as

$$81 \quad \eta_{e,uncor} = \frac{P_{sub}}{P_{rf} + cP_i} = \frac{P_{sub}}{P_{sub} + P_w + cP_i} = \frac{P_{sub}}{P_{sub} + \frac{\Delta e}{k}}. \quad (4)$$

82 The correction factor  $g$  of a microcalorimeter is then defined as,

$$83 \quad g = \frac{\eta_e}{\eta_{e,uncor}} = 1 + \frac{cP_i}{P_{rf}}. \quad (5)$$

84 The correction factor  $g$  is used to remove the contribution of  $P_i$  from the directly calculated  
 85 uncorrected effective efficiency  $\eta_{e,uncor} = \left[1 - \left(\frac{V_2}{V_1}\right)^2\right] / \left[\frac{e_2}{e_1} - \left(\frac{V_2}{V_1}\right)^2\right]$  [7, 12] with the measured  $V_1$ ,  $V_2$ ,  
 86  $e_1$  and  $e_2$  using the hardware setup in Figure 1.

## 87 2.2. System Constant

88 For a thermistor mount with input reflection coefficient of  $\Gamma_M$  and incident power of  $P_{IM}$ , the  
 89 dissipated power  $P_i$  at the TIS due to both the forward and reverse transmissions is,

$$90 \quad P_i \cong k_i(1 + |\Gamma_M|^2)P_{IM}, \quad (6)$$

91 where  $k_i$  is the power dissipation coefficient of TIS. The net absorbed power by the thermistor mount  
 92 is

$$93 \quad P_{rf} = (1 - |\Gamma_M|^2)P_{IM}. \quad (7)$$

94 Therefore, it can be obtained from (5)-(7) that

$$95 \quad g = 1 + ck_i \frac{1 + |\Gamma_M|^2}{1 - |\Gamma_M|^2}. \quad (8)$$

96 Since  $c$  and  $k_i$  are determined by the physical structure and the material property of a waveguide  
 97 TIS, their product  $ck_i$  is actually a system constant of the microcalorimeter and denoted as  $\varphi$  in this  
 98 study. From (8), it is clearly noted that once the system constant  $\varphi = ck_i$  is obtained, the correction  
 99 factor  $g$  of microcalorimeter for calibrating a thermistor mount with known input reflection  
 100 coefficient  $\Gamma_M$  can be determined, and thereby the effective efficiency  $\eta_e$  of the thermistor mount.

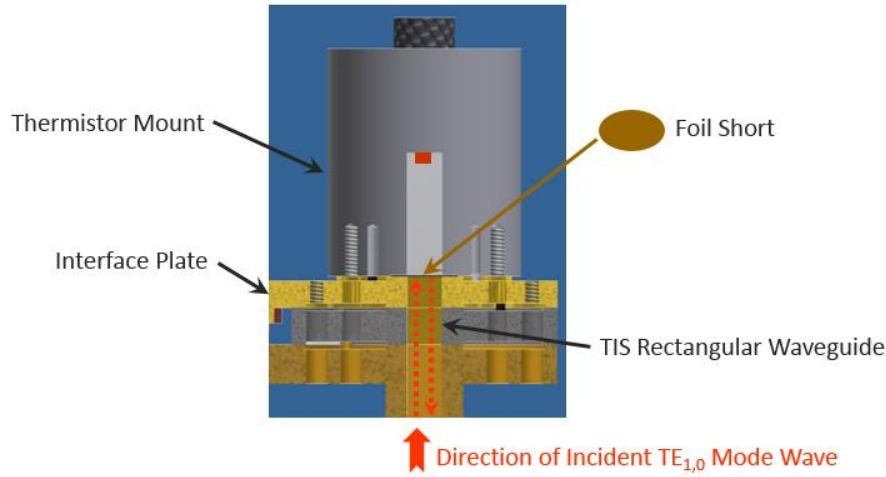
## 101 3. Determination of the Correction Factor

102 “Foil Short” measurement has been well-accepted for experimental determination of the  
 103 correction factor  $g$  [7, 11]. A schematic illustration of “Foil Short” measurement is shown in Figure 2  
 104 as a reference, where a foil short is inserted between the DUT (thermistor mount) to be calibrated and  
 105 the interface plate. During the “Foil Short” measurements, the DUT is dc-biased through the Type-  
 106 IV power meter in a steady status.

107 With the RF input on, the power  $P_{FS}$  dissipated at the foil short and the power  $P_{i,FS}$  dissipated  
 108 at the TIS cause the output voltage change  $\Delta e_{FS}$  of the thermopile. Similar to (3), the following  
 109 relationship can be arrived

$$110 \quad \Delta e_{FS} = k(P_{FS} + cP_{i,FS}). \quad (9)$$

111



112

113 **Figure 2.** Concept of “Foil Short” measurements for determining the correction factor of a waveguide  
114 microcalorimeter.

115 For the foil short with a reflection coefficient of  $\Gamma_{FS}$  and incident power of  $P_{IFS}$  to the TIS,  
116 similar to (6), the dissipated power  $P_{i,FS}$  at the TIS can be determined as

$$117 \quad P_{i,FS} \cong k_i(1 + |\Gamma_{FS}|^2)P_{IFS}. \quad (10)$$

118 Combining (9) and (10), it can be obtained that

$$119 \quad \varphi = ck_i = \frac{\Delta e_{FS}}{k(1 + |\Gamma_{FS}|^2)P_{IFS}} - \frac{P_{FS}}{(1 + |\Gamma_{FS}|^2)P_{IFS}}. \quad (11)$$

120 Since  $P_{FS} = P_{IFS}(1 - |\Gamma_{FS}|^2)$ , conventionally combining (8) and (11), the correction factor  $g$  of a  
121 microcalorimeter can be determined as

$$122 \quad g = 1 + \frac{\Delta e_{FS}}{k(1 + |\Gamma_{FS}|^2)P_{IFS}} \times \frac{1 + |\Gamma_M|^2}{1 - |\Gamma_M|^2} - \frac{1 - |\Gamma_{FS}|^2}{1 + |\Gamma_{FS}|^2} \times \frac{1 + |\Gamma_M|^2}{1 - |\Gamma_M|^2}. \quad (12)$$

123

124 This relationship has been reported in [7, 11–12]. However, a recent bilateral comparison [14] of  
125 scattering parameter magnitude measurements of WR-15 (50–75 GHz) and WR-10 (75–110 GHz)  
126 waveguide type between the Istituto Nazionale di Ricerca Metrologica (INRIM), Italy and the  
127 National Metrology Center, A\*STAR (NMC), Singapore showed that the uncertainty of reflection  
128 coefficient for a “Short” traveling standard can vary from 0.005 to 0.02 (at a 95% confidence level).  
129 Higher uncertainty of the reflection coefficient  $\Gamma_{FS}$  for foil short can then be propagated to the  
130 estimated correction factor  $g$ , and thereby the determined effective efficiency  $\eta_e$ . Therefore, it  
131 motivates us to find an alternative solution for determining the correction factor  $g$  as discussed below.

132 Through re-organizing (11), we can achieve that

$$133 \quad \varphi = \frac{\Delta e_{FS}}{k(1 + |\Gamma_{FS}|^2)P_{IFS}} \left( 1 - \frac{kP_{FS}}{\Delta e_{FS}} \right). \quad (13)$$

134 With (9), it is found that

$$135 \quad \varphi = \frac{\Delta e_{FS}}{k(1 + |\Gamma_{FS}|^2)P_{IFS}} \left( \frac{c}{\frac{P_{FS}}{P_{i,FS}} + c} \right). \quad (14)$$

136 In this study, a power ratio  $\rho$  between  $P_{FS}$  and  $P_{i,FS}$  is defined as  $\rho = P_{FS}/P_{i,FS}$ , then we can  
137 get

$$138 \quad \varphi = \frac{c}{c + \rho} \times \frac{\Delta e_{FS}}{k(1 + |\Gamma_{FS}|^2)P_{IFS}}. \quad (15)$$

139 Combining (15) with (8), a new correction factor  $g$  is proposed in this study for evaluating the  
 140 waveguide microcalorimeter as follows,

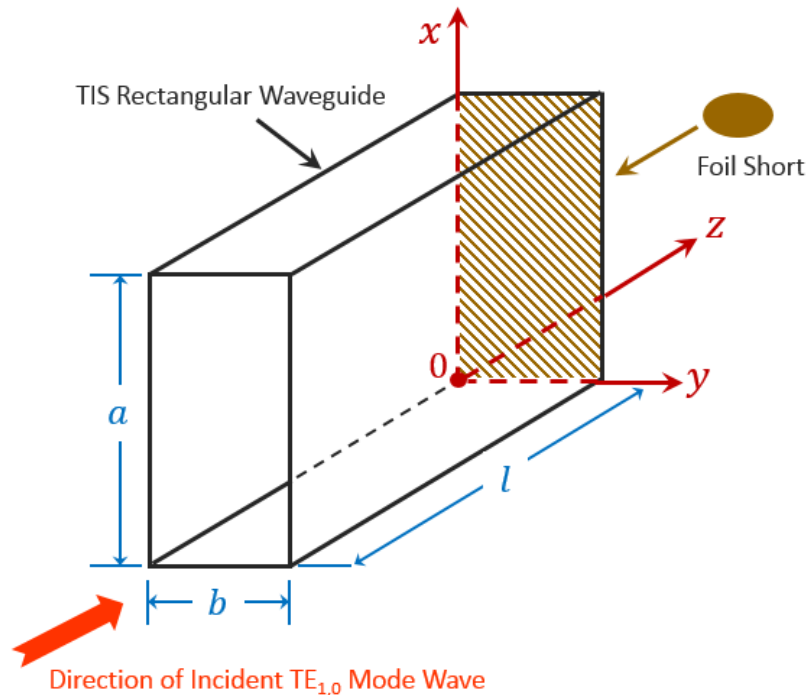
$$141 \quad g = 1 + \frac{c}{c + \rho} \times \frac{\Delta e_{FS}}{k(1 + |\Gamma_{FS}|^2)P_{IFS}} \times \frac{1 + |\Gamma_M|^2}{1 - |\Gamma_M|^2}. \quad (16)$$

142 Here, it needs to highlight that significant uncertainty portion involving  $\Gamma_{FS}$  and  $\Gamma_M$  as underbraced  
 143 in (12) has been eliminated in (16), but with the introduction of another factor determined by power  
 144 ratio  $\rho$  and equivalence factor  $c$  which may be under control better. This proposed solution in (16)  
 145 theoretically may offer a smaller combined uncertainty. The equivalence factor  $c$  that considers the  
 146 thermal paths which are different comparing to those from the thermistor mount to the thermopile  
 147 approximates to be 0.5 (as representative of all the microcalorimeters in [7]). This is because the  
 148 relative heating effectiveness through the TIS changes linearly from a value of approximately one at  
 149 the mount flange to almost zero at the far end as discussed in [7]. As a result, only half of the heating  
 150 in the TIS is measured by the thermopile.

151 Therefore, proper determination of the power ratio  $\rho$  between  $P_{FS}$  (the power dissipated at the  
 152 foil short) and  $P_{i,FS}$  (the power dissipated at the TIS) in “Foil Short” measurements becomes very  
 153 important for evaluating the system constant  $\varphi$  of a waveguide microcalorimeter, and thereby its  
 154 correction factor  $g$  for calibrating the thermistor mounts. In the following section, we propose to  
 155 apply the electromagnetic field theory analysis to determine this power ratio theoretically in this  
 156 study.

#### 157 4. Mathematical Modelling Through Electromagnetic Field Theory Analysis

158 The properties of waveguides in support of wave propagation and mode are characterized by  
 159 the presence of longitudinal magnetic or electric field components, and can be derived by  
 160 electromagnetic field theory analysis [15, Ch. 3].



161

162

**Figure 3.** Dimensional illustration of TIS with incident  $TE_{1,0}$  mode wave in “Foil Short” measurement.

163 In a rectangular waveguide, the dominant wave propagating inside is the TE<sub>1,0</sub> mode. In the  
 164 following analysis, it is assumed that both the waveguide walls and the foil short have high  
 165 conductivity  $\sigma$  and small skin depth  $\delta$  resulting in small losses (almost lossless, with attenuation  
 166 constant  $\alpha \approx 0$ ) which do not appreciably perturb the TE<sub>1,0</sub> mode fields. For the incident wave in + z  
 167 direction with a peak amplitude level of  $A$ , and with a foil short at  $z = 0$  along the rectangular  
 168 waveguide ( $a > b$ ) as shown in Figure 3, the transverse field components are

$$169 \left\{ \begin{array}{l} H_z = A \left\{ \cos\left(\frac{\pi x}{a}\right) \right\} (1 + \Gamma_z e^{j2\beta z}) e^{-j\beta z}, \\ H_x = j \frac{\beta}{K_c} A \left\{ \sin\left(\frac{\pi x}{a}\right) \right\} (1 - \Gamma_z e^{j2\beta z}) e^{-j\beta z}, \\ E_y = -j \frac{\beta}{K_c} Z_h A \left\{ \sin\left(\frac{\pi x}{a}\right) \right\} (1 + \Gamma_z e^{j2\beta z}) e^{-j\beta z}, \\ E_x = E_z = H_y = 0, \end{array} \right. \quad (17)$$

170 where  $K_c$  is the cutoff wave number,  $\beta$  is the phase constant, and  $Z_h$  is the wave impedance, as  
 171 follows,

$$172 K_c = \frac{\pi}{a}, \beta = \frac{2\pi}{\lambda_g}, \text{ and } Z_h = \eta \frac{\lambda_g}{\lambda}.$$

173 Here,  $\lambda_g$  is the guide wavelength and equal to,

$$174 \lambda_g = \frac{\lambda}{\sqrt{1 - \left(\frac{\lambda}{2a}\right)^2}}$$

175 for the wavelength  $\lambda$  in TE<sub>1,0</sub> mode.  $\Gamma_z$  is the voltage reflection coefficient at  $z = 0$  (approximately -1  
 176 for the foil short) as shown in Figure 3. The incident power  $P_{IFS}$  (at  $z = 0$ ) is

$$177 P_{IFS} = \frac{1}{2} \text{Re} \int_0^{x=a} \int_0^{y=b} \vec{E} \times \vec{H}^* \cdot \hat{z} \, dx \, dy = \frac{1}{2} \left(\frac{\beta}{K_c}\right)^2 Z_h A^2 \frac{ab}{2}. \quad (18)$$

178 For convenient in calculation, eq. (17) can be reformatted as [16]

$$179 \left\{ \begin{array}{l} H_z = -2jA \cos\left(\frac{\pi x}{a}\right) \sin \beta z, \\ H_x = 2j \frac{\beta}{K_c} A \sin\left(\frac{\pi x}{a}\right) \cos \beta z, \\ E_y = -2 \frac{\beta}{K_c} Z_h A \sin\left(\frac{\pi x}{a}\right) \sin \beta z. \end{array} \right. \quad (19)$$

180 It is noted that the dissipated power  $P_s$  at a wall surface with surface resistance  $R_s$  is

$$181 P_s \\ 182 = \frac{R_s}{2} \iint \vec{J}_s \\ 183 \times \vec{J}_s^* \, dA, \quad (20)$$

184 where the surface current density  $\vec{J}_s$  is given by

$$185 \vec{J}_s \\ 186 \cong \hat{n} \\ 187 \times \vec{H}_{surface}. \quad (21)$$

188 Therefore for the broad wall ( $a$  by  $l$ ) as shown in Figure 3, the magnitudes of the  $x$  and  $z$   
 189 component of the current densities are

$$190 |J_x| \cong 2A \cos\left(\frac{\pi x}{a}\right) \sin \beta z, \quad (22)$$

191  $|J_z| \cong 2 \left( \frac{\beta}{K_c} \right) A \sin \left( \frac{\pi x}{a} \right) \cos \beta z.$  (23)

192 The magnitudes of the current density in the narrow wall ( $b$  by  $l$ ) is

193  $|J_{NW}| \cong 2A \sin \beta z.$  (24)

194 The magnitudes of the current density in the foil short ( $a$  by  $b$ ) is

195  $|J_{FS}| \cong 2 \left( \frac{\beta}{K_c} \right) A \sin \left( \frac{\pi x}{a} \right).$  (25)

196 According to (20), the power  $P_{BW}$  dissipated in the two broad walls is

197 
$$P_{BW} = 2 \cdot \frac{R_S}{2} \int_0^{x=a} \int_0^{z=l} (|J_x|^2 + |J_z|^2) dx dz \cong A^2 \frac{al}{\sigma \delta} \left\{ 1 + \left( \frac{\beta}{K_c} \right)^2 \right\} .$$
 (26)

198 Similarly, the power  $P_{NW}$  dissipated in the two narrow walls is

199 
$$P_{NW} = 2 \cdot \frac{R_S}{2} \int_0^{y=b} \int_0^{z=l} |J_{NW}|^2 dy dz = 4A^2 \frac{bl}{\sigma \delta} \left\{ \frac{1}{2} - \frac{\sin 2\beta l}{\beta l} \right\} \cong 2A^2 \frac{bl}{\sigma \delta},$$
 (27)

200 and the power  $P_{FS}$  dissipated in the foil short is

201 
$$P_{FS} = \frac{R_S}{2} \int_0^{x=a} \int_0^{y=b} |J_{FS}|^2 dx dy = \left( \frac{\beta}{K_c} \right)^2 A^2 \frac{ab}{\sigma \delta} .$$
 (28)

202 Therefore,

203 
$$\rho = \frac{P_{FS}}{P_{i,FS}} = \frac{P_{FS}}{P_{BW} + P_{NW}} = \frac{\left( \frac{\beta}{K_c} \right)^2 ab}{2bl + al \left\{ 1 + \left( \frac{\beta}{K_c} \right)^2 \right\}} = \frac{\left( \frac{2a}{\lambda_g} \right)^2 ab}{2bl + al \left\{ 1 + \left( \frac{2a}{\lambda_g} \right)^2 \right\}} .$$
 (29)

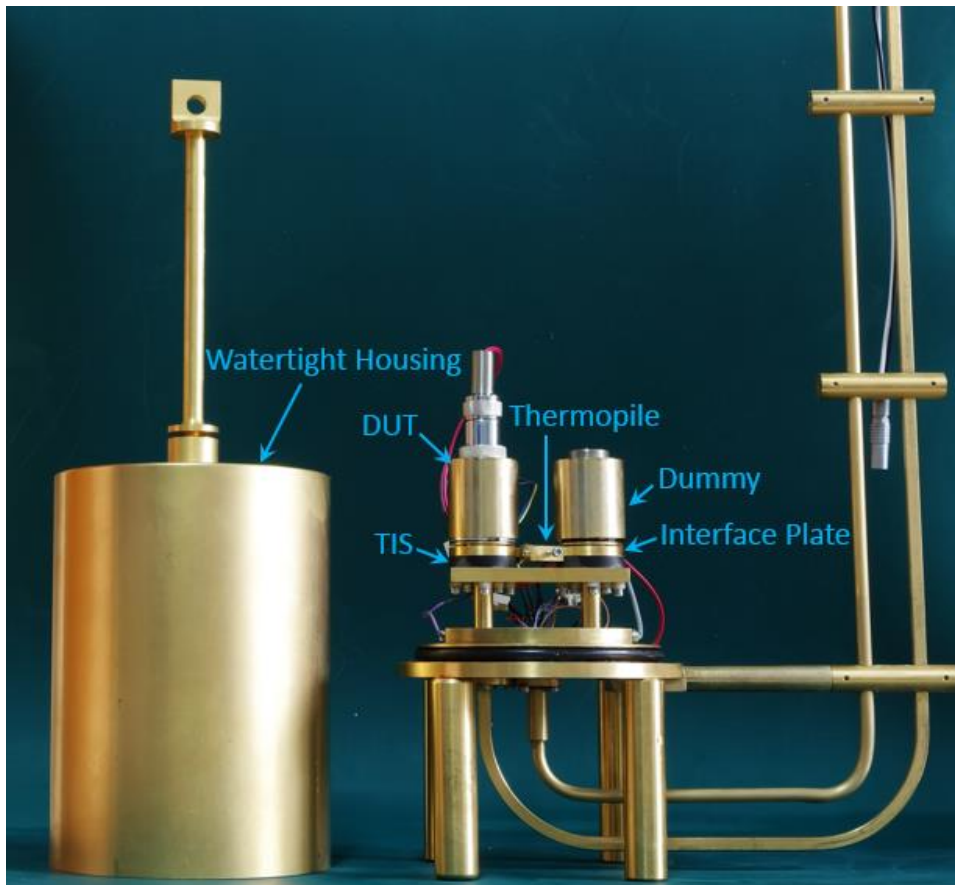
204 Here, it needs to be highlighted that final expression in (29) is achieved with the elimination of the  
 205 surface resistance  $R_s$  at both the denominator and numerator. This elimination/simplification is  
 206 valid only under the assumption that the TIS and the foil short share the same (or approximately the  
 207 same) electrical characteristics such as conductivity  $\sigma$  and skin depth  $\delta$ , and if the metal thickness  
 208 is higher than the skin depth for both the TIS and the foil short.

209 In practical, these requirements could be achieved during the fabrication of TIS and foil short,  
 210 using the same metal material with enough thickness and with same surface treatment. Together with  
 211 (16), the correction factor  $g$  can be determined properly using (29). In the next section, its performance  
 212 will be compared with conventional method with detailed discussion.

## 213 5. Performance Evaluation and Analysis

214 Performance of the newly proposed correction factor  $g$  in (16) has been evaluated with a WR-15  
 215 microcalorimeter that is now serving as the national waveguide primary power standard of China.  
 216 Figure 4 below shows an assembled WR-15 microcalorimeter that will be used in the evaluation,  
 217 which covers the frequency range of 50–75 GHz.

218



219

220

221

**Figure 4.** Picture of a WR-15 (50-75 GHz) microcalorimeter assembled at the National Institute of Metrology, China.

222

*5.1. Performance Evaluation of the Proposed Correction Factor  $g$*

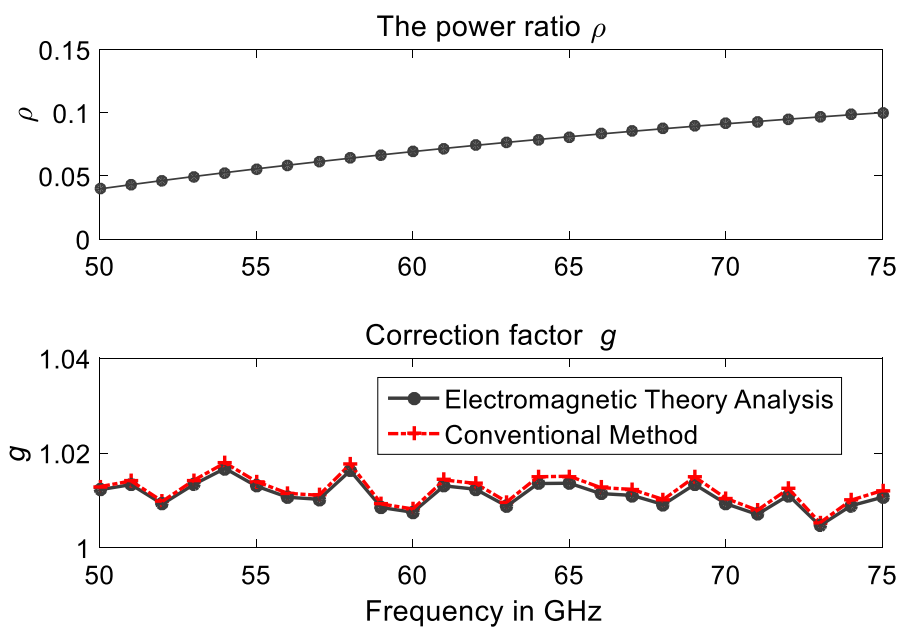
223

224

225

226

The TIS of the fabricated microcalorimeter has dimensions of  $a = 0.00376$  m,  $b = 0.00188$  m, and  $l = 0.0105$  m. It is noted that the interface plate as shown in Figure 4 has an exactly same size as the TIS.



227



228 **Figure 5.** Results of power ratio  $\rho$ , and comparison of correction factor  $g$  for the WR-15  
 229 microcalorimeter using the conventional method and the proposed method with electromagnetic  
 230 field theory analysis.

231 Figure 5 presents the experimental results of  $\rho$  and the estimated correction factor  $g$  covering the  
 232 whole frequency band (50–75 GHz) for the fabricated WR-15 microcalorimeter shown in Figure 4,  
 233 using the proposed method (eq. (16)) and the conventional method (eq. (12)). From Figure 5, it can be  
 234 found that good agreements between the results for correction factor  $g$  from the electromagnetic  
 235 theory analysis and from the conventional method can be achieved. The proposed method with  
 236 electromagnetic theory analysis is then used for evaluating the WR-15 microcalorimeter at the  
 237 National Institute of Metrology, China. Detailed analysis with uncertainty evaluation are discussed  
 238 below.

239 **Table 1.** Uncertainty budget for correction factor at 72 GHz.

Quantity	Uncertainty Components	Type	Probability Distribution	Standard Uncertainty $u_i(x)$	Sensitivity Coefficient $c_i$	$u_i(y) = c_i u_i(x)$
$\rho$	Caliper	B	Rectangular	0.0005	-0.01371	-0.000007
$P_1$	Digital multimeter	B	Rectangular	0.001	0.00070	0.000001
$e_1$	Digital voltmeter	B	Rectangular	0.04	-0.00002	-0.000001
$\Delta e_{FS}$	Digital voltmeter	B	Rectangular	0.08	0.01520	0.001216
$\Gamma_{FS}$	Network analyzer	B	Rectangular	0.01	-0.01502	-0.000150
$P_{IFS}$	Type IV power meter & Digital voltmeter	B	Rectangular	0.08	-0.01683	-0.001347
$\Gamma_M$	Network analyzer	B	Rectangular	0.01	0.00777	0.000078
$g$	Repeatability (Typical)	A	Normal	0.001	1	0.001
Combined Standard Uncertainty for Correction Factor $g$ at 72 GHz						0.002

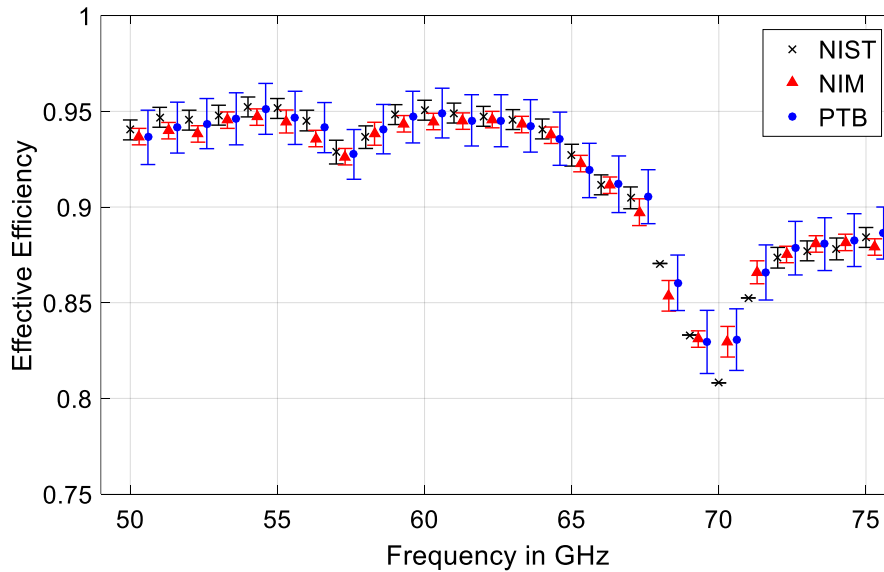
## 240 5.2. Uncertainty Evaluation

241 Table 1 shows one example for evaluating the measurement uncertainty of the correction factor  
 242  $g$  of a reference standard (Hughes 45774H-1100 thermistor power sensor), using the proposed  
 243 method (eq. (16)) at 72 GHz.  $P_1$  and  $e_1$  are the DC-biased power and the output voltage of  
 244 thermopile without RF input respectively, and they are used to experimentally determine  $k$ , the  
 245 proportionality constant that depends on the fraction of power flowing through the thermopile and  
 246 the thermopile sensitivity [11]. The calculated combined standard uncertainty for correction factor  $g$   
 247 at 72 GHz is around 0.002, following the “Guide to the Expression of Uncertainty in Measurement” (GUM)  
 248 [17].

249 To obtain the measurement uncertainty  $\Delta\eta_e$  for the effective efficiency  $\eta_e$  ( $\eta_e = g \cdot \eta_{e,uncor}$ ) of  
 250 the thermistor mount under test, it can arrive that

$$251 \Delta\eta_e = \sqrt{\left(\frac{\partial\eta_e}{\partial g}\right)^2 \Delta g^2 + \left(\frac{\partial\eta_e}{\partial\eta_{e,uncor}}\right)^2 \Delta\eta_{e,uncor}^2} \quad (30)$$

252 The uncertainty for the uncorrected effective efficiency  $\eta_{e,uncor}$  was evaluated in the conventional  
 253 way, and found to be 0.0013 at 72 GHz. Using (30), it is found that the combined standard uncertainty  
 254 for the effective efficiency of the thermistor mount under test at 72 GHz is 0.0024. That is, the  
 255 expanded uncertainty is approximately 0.0048 at a level of confidence of approximately 95%  
 256 assuming a Gaussian distribution.



257

258

259

260

261

**Figure 6.** Measured results of the effective efficiency  $\eta_e$  for a Hughes 45774H-1100 thermistor power sensor at different laboratories for performance comparison. Uncertainty bars are shown at a level of confidence of approximately 95% assuming a Gaussian distribution. Frequency values are shifted for better readability and no uncertainty value provided by NIST for 68, 69, 70 and 71 GHz.

262

### 5.3. International Comparison

263

264

265

266

267

268

269

270

271

272

273

274

275

To further evaluate the performance of the proposed method (eq. (16)) with the newly fabricated WR-15 microcalorimeter shown in Figure 4, an informal international comparison [18] of WR-15 (50 to 75 GHz) power measurements has been arranged among at the National Institute of Metrology (NIM) of China, the National Institute of Standards and Technology (NIST) of USA, the Physikalisch-Technische Bundesanstalt (PTB) of Germany, and the National Metrology Centre (NMC) of Singapore.

Comparison results of the measured effective efficiency for one of the traveling standards, Hughes 45774H-1100 thermistor power sensors are presented in Figure 6 for the whole frequency range of 50–75 GHz, using the proposed method in this paper and also compared to the primary power measurement systems at NIST and PTB. From the results, good equivalence of power measurements in WR-15 waveguide has been clearly observed among the participating laboratories. This further validates the proposed method and newly developed primary power measurement system at the NIM, China, for calibrating the waveguide RF power sensors.

276

## 5. Conclusions

277

278

279

280

281

282

283

284

285

286

287

288

289

In this paper, a new method for determining the correction factor  $g$  of a waveguide microcalorimeter was reported, using the electromagnetic field theory to analysis the effect of waveguide TIS in “foil short” measurement mode. The proposed method determines the contribution of the power dissipated within the TIS into the correction factor  $g$ , in term of the physical dimensions of the TIS.

The proposed method has been implemented to evaluate a newly fabricated WR-15 microcalorimeter at the NIM, China. The estimated correction factor  $g$  of the microcalorimeter using the proposed method has been compared against the conventional method, and good agreements have been observed. To further evaluate its performance, the proposed method with the newly fabricated WR-15 microcalorimeter has been evaluated in an informal international comparison of WR-15 (50 to 75 GHz) power measurements with the NIST of USA, the PTB of Germany and the NMC of Singapore, where good equivalence has been observed.

290 **Author Contributions:** Conceptualization, X.C., W.Y. and Y.L.; methodology, X.C. and Y.L.; software, W.Y.;  
291 validation, X.C., Y.S.M., W.Y. and Y.L.; formal analysis, X.C., Y.S.M. and W.Y.; investigation, X.C., Y.S.M., W.Y.  
292 and Y.L.; resources, X.C.; writing—original draft preparation, X.C. and Y.S.M.; writing—review and editing, X.C.  
293 and Y.S.M.; visualization, X.C., Y.S.M. and W.Y.; supervision, X.C.; project administration, X.C.; funding  
294 acquisition, X.C..

295 **Funding:** This work was funded in part by the National Science and Technology Supporting Program entitled  
296 Terahertz Wave WR-3 (220 GHz to 330 GHz) Power Primary Standard, China, under Grant No. 2018YFF0212101.  
297 Y. S. Meng was supported by the Overseas Experts Supporting Program of the State Administration of Foreign  
298 Experts Affairs, China.

299 **Conflicts of Interest:** The authors declare no conflict of interest.

## 300 References

- 301 1. Fantom, A. *Radio Frequency and Microwave Power Measurement*, Peter Peregrinus Ltd.: Stevenage, U.K., 1990.
- 302 2. Neji, B.; Xu, J.; Titus, A.H.; Meltzer, J. Micro-fabricated DC comparison calorimeter for RF power  
303 measurement. *Sensors* **2014**, *14*, 20245–20261.
- 304 3. Martinovic, Z.; Dadic, M.; Ivisic, B.; Malaric, R. An adiabatic coaxial line for microcalorimeter power  
305 measurements in wireless communication for smart grid. *Energies* **2019**, *12*, 4194.
- 306 4. Engen, G. F. A refined X-band microwave microcalorimeter. *J. Res. Nat. Bur. Stand.* **1959**, *63C*, 77–82.
- 307 5. Chung, N. S.; Sin, J.; Bayer, H.; Honigbaum, R. Coaxial and waveguide microcalorimeters for RF and  
308 microwave power standards. *IEEE Trans. Instrum. Meas.* **1989**, *38*, 460–464.
- 309 6. Kang, T. W.; Chung, N. S.; Honigbaum, R.; Rühaak, J.; Stumper, U. K- and Ka-band waveguide  
310 microcalorimeters for microwave power standards. *IEEE Trans. Instrum. Meas.* **1997**, *46*, 1247–1250.
- 311 7. Allen, J. W.; Clague, F. R.; Larsen, N. T.; Weidman, M. P. NIST microwave power standards in waveguide.  
312 *NIST Tech. Note 1511*. **1999**.
- 313 8. Shimaoka, K.; Kinoshita, M.; Inoue, T. A broadband waveguide calorimeter in the frequency range from 50  
314 to 110 GHz. *IEEE Trans. Instrum. Meas.* **2013**, *62*, 1828–1833.
- 315 9. Clague, F. R. A method to determine the calorimetric equivalence correction for a coaxial microwave  
316 microcalorimeter. *IEEE Trans. Instrum. Meas.* **1994**, *43*, 421–425.
- 317 10. Judaschke, R.; Ruhaak, J. Determination of the correction factor of waveguide microcalorimeters in the  
318 millimeter-wave range. *IEEE Trans. Instrum. Meas.* **2009**, *58*, 1104–1108.
- 319 11. Cui, X.; Crowley, T. P. Comparison of experimental techniques for evaluating the correction factor of a  
320 rectangular waveguide microcalorimeter. *IEEE Trans. Instrum. Meas.* **2011**, *60*, 2690–2695.
- 321 12. Cui, X.; Meng, Y. S.; Li, Y.; Zhang, Y.; Shan, Y. An improved design and simplified evaluation technique  
322 for waveguide microcalorimeter. *IEEE Trans. Instrum. Meas.* **2016**, *65*, 1450–1455.
- 323 13. Cui, X.; Meng, Y. S.; Li, Y.; Yuan, W.; Ma, C.; Shan, Y. Comparative modeling of thermal isolation section  
324 in a rectangular waveguide microcalorimeter. In Proceedings of the Conference on Precision  
325 Electromagnetic Measurements, Ottawa, Canada, 10–15 July 2016.
- 326 14. Sellone, M.; Oberto, L.; Shan, Y.; Meng, Y. S.; Brunetti, L.; Shoaib, N. Comparison of S-Parameter  
327 measurements at millimeter wavelengths between INRIM and NMC. *IEEE Trans. Instrum. Meas.* **2014**, *63*,  
328 1810–1817.
- 329 15. Pozar, D. M. *Microwave Engineering*, Addison-Wesley: Reading, MA, USA, 1993.
- 330 16. Beatty, R. W. Applications of waveguide and circuit theory to the development of accurate microwave  
331 measurement methods and standards. *Nat. Bur. Stand. (U.S.A), Monogr.* **1973**, *137*.
- 332 17. BIPM; IEC; IFCC; ILAC; ISO; IUPAC; IUPAP; OIML. Evaluation of Measurement Data—Guide to the  
333 Expression of Uncertainty in Measurement. *JCGM 100:2008 (GUM 1995 with minor corrections)*. **2008**, Joint  
334 Committee for Guides in Metrology. Available: <http://www.bipm.org/en/publications/guides/gum.html>
- 335 18. Cui, X.; Meng, Y. S.; Judaschke, R.; Ruhaak, J.; Crowley, T. P.; Ginley, R. A. International comparison of  
336 WR15 (50 to 75 GHz) power measurements among NIST, NIM, PTB and NMC, A\*STAR. In Proceedings of  
337 the Conference on Precision Electromagnetic Measurements, Ottawa, Canada, 10–15 July 2016.
- 338



© 2019 by the authors. Submitted for possible open access publication under the terms and conditions of the Creative Commons Attribution (CC BY) license (<http://creativecommons.org/licenses/by/4.0/>).